

3. Investigation of the Mechanisms of Inter- and Intramolecular Disulfide Bond Cleavages in Model Peptides by Covalently Attached Acetyl Radical

Abstract We investigate the mechanism of disulfide bond cleavage in gaseous peptide ions triggered by a regiospecific covalently attached acetyl radical. We describe a second generation 2,2,6,6-tetramethylpiperidine-1-oxyl (TEMPO)-based free radical initiated peptide sequencing (FRIPS) reagent (**10**) that yields acetyl radical peptide ions in a single step of collisional activation. Derivatized model peptide ions containing inter- or intramolecular disulfide bonds are collisionally activated to yield an N-terminal acetyl radical group via loss of TEMPO radical. Further collisional activation of the acetyl radical peptide results in highly selective C–S and S–S bond cleavages. To probe their mechanisms, model peptides having a deuterated β -carbon at the disulfide bond are employed. It is suggested that the major pathway of S–S bond cleavage is triggered by hydrogen abstraction from the α -carbon, followed by radical substitution to the S–S bond, yielding thiirane and thiyl radical products. A minor contribution by direct radical substitution to the disulfide bond is also considered. Density functional theory calculations are performed to explore energetics of the proposed mechanisms for disulfide bond cleavage.

3.1. Introduction

As an important post-translational modification, identification and characterization of disulfide bonds in proteins are critical for their three-dimensional structure determination.¹⁵² The disulfide bond, a strong covalent linking of two cysteine residues between protein subunits, contributes significantly to stabilization of tertiary protein structures^{153,154} and helps to maintain protein activity in cellular environments.¹⁵⁵⁻¹⁵⁸ Despite their important role, analysis of disulfide bonds in

proteins remains a challenging task exacerbated by their fragility toward redox stress. The native disulfide connectivity can be easily lost by reduction and re-oxidation of disulfides, which may occur randomly during sample preparation for analysis. To avoid this problem, pretreatment of disulfides by reduction and alkylation is often performed, with concomitant loss of important structural information.¹⁵⁹

Not surprisingly, the rapid expansion of experimental methodology employing high performance mass spectrometry (MS) in protein identification and structural determination has included the development of new approaches for disulfide bond characterization.¹⁶⁰ Low-energy collisional activation of protonated peptides containing disulfide bonds usually leads to a mixture of amide backbone and disulfide C–S bond cleavage, with essentially no S–S bond rupture due to the higher activation energy required for this process.¹⁶¹ Protein digests generated by proteases that retain intact disulfide bonds typically contain both inter- and intramolecular disulfide linkages. Cleavage of intermolecular disulfide bonds leads to separated peptide fragments and further collisional activation can yield fragments revealing the point of connection. Intramolecular disulfide bonds require multiple steps of activation to locate the linkage sites. Therefore, only limited structural information can be acquired by conventional low-energy collision induced dissociation (CID) of protonated peptides containing intramolecular disulfide bonds.¹⁶² Some of the low-energy CID approaches with certain limited conditions generate more information-rich fragments. Gaseous peptide ions lacking mobile protons typically exhibit highly selective C–S bond cleavages by low-energy CID.¹⁶³ This effect is especially prominent in singly protonated disulfide containing peptide ions produced by matrix-assisted laser desorption ionization (MALDI).¹⁶⁴ CID of anionic disulfide-bridged peptides also generates cleavage products from C–S bond fragmentation but their intensities are usually weak and the pattern of fragmentation is complex.¹⁶⁵⁻¹⁶⁷

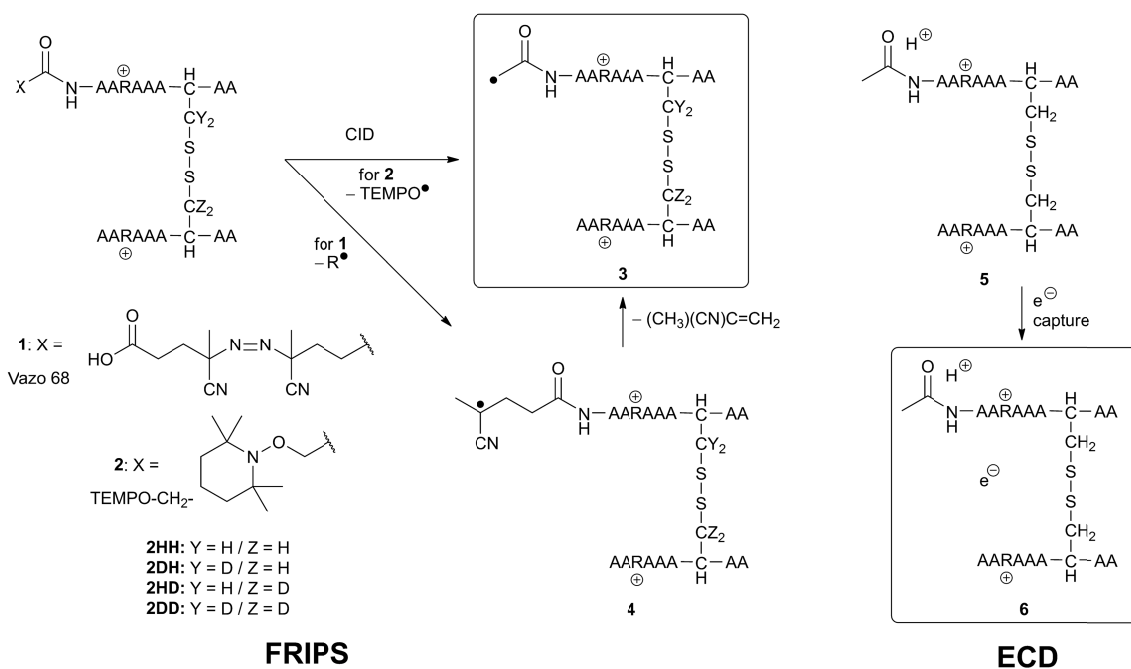
Metal cationized disulfide containing peptides have also been thoroughly investigated by MS. The patterns of disulfide fragmentation with various metal complexes under low-energy CID are diverse.¹⁶⁸ For example, disulfide bond containing peptides cationized by a gold cation undergo efficient S–S bond cleavages by low-energy CID.¹⁶⁹ Alkali or alkaline earth metal–peptide complexes cleave C–S bonds, yielding highly selective H₂S₂ loss.^{39,40} This signature neutral loss can be used for fast screening of disulfide containing peptides in complex mixtures, including those resulting from peptic digests.^{39,40} The observed processes are triggered by anionic enolation of cysteine residues at backbone C_α positions by metal cations, followed by sequential cleavage of the C–S bonds.

Electron capture dissociation (ECD)¹³ and its variation, electron transfer dissociation (ETD)¹⁴, have been very attractive methods for analysis of disulfide linkages, deriving advantage from selective cleavage of S–S bonds in peptides and proteins.⁵³ In ECD and ETD, the ion activation occurs via electron capture or transfer to multiply charged peptide cations, followed by electronic state relaxation via internal conversion.¹⁷⁰ Initially, dissociative addition of a hydrogen atom to the disulfide bond was suggested to explain the selective S–S bond fragmentation (the Cornell mechanism).^{53,171} Direct electron capture or intramolecular electron transfer from high-lying orbitals to the Coulomb stabilized σ^* orbital of the S–S bond were alternatively proposed.^{72,74,76,77,79,80,172,173} Even when all charged sites in the peptide cations are fixed-charge groups such as quaternary ammoniums, S–S bond cleavage is still observed in the absence of a mobile hydrogen atom.¹⁰⁰ This observation supports an alternative mechanistic viewpoint, in which the Coulomb stabilization between positively charged sites and disulfide bonds promotes exothermic intramolecular electron transfer to the σ^* orbital of the S–S bond (mainly the Utah part in the Utah-Washington mechanism). The detailed processes for initial electron capture and

subsequent S–S bond cleavage in various disulfide bond containing peptides and proteins remain an active subject for further experimental and theoretical investigations.¹⁷⁴

We have previously described a method for free radical initiated peptide sequencing (FRIPS) via multistep collisional activation of peptides conjugated with a reagent (Vazo 68, **Scheme 3.1**) that introduces a regiospecific free radical center.¹⁵ FRIPS of peptide conjugates can effect backbone fragmentation, producing mainly a- or x- and z-type ions whose charges are located at the N- or C-terminal sides of peptides, respectively. These fragment ions are not usually observed in low-energy CID spectra of protonated peptide cations. The radical center produced by FRIPS typically reacts by H-atom abstraction either from α - or β -carbons, followed by β -cleavage. This leads primarily to side-chain loss and backbone fragmentation, respectively.

In this paper, we apply our FRIPS methodology to characterize disulfide bond connectivity in peptides and their mechanisms of disulfide bond cleavages are investigated. In addition, we compare and contrast the distinctly different processes associated with FRIPS and ECD that trigger radical-driven cleavages in the gas phase. Our earlier study employed Vazo 68, a commercially available water soluble free-radical initiator, conjugated to the peptide N-terminus to induce hydrogen deficient radical-driven fragmentations (**Scheme 3.1, 1**).¹⁵



Scheme 3.1

Upon sequential collisional activation, a regiospecific acetyl radical group (**3**) is produced, which abstracts C_α and C_β hydrogens with concomitant β-cleavage to yield mainly side-chain losses and backbone fragmentations, respectively. In the present study, we employ a second generation FRIPS reagent (**Scheme 3.2**, **10**) inspired by Lee *et al.*¹⁷⁵ The peptide sequencing performance of this reagent is validated with model peptides including the tryptic peptide, HSDAVFTDNYTR, the intramolecular disulfide bond containing peptides, Arg8-Vasopressin, and Arg8-Conopressin G, and the intermolecular disulfide bond containing peptide from a tryptic digest of Arg8-Conopressin G (**Scheme 3.4**). To probe the mechanisms of disulfide bond cleavages, the model peptides having one or two β-deuterium(s) at the disulfide bond are employed (**Scheme 3.1**, **2** with no deuterium (**2HH**), β-deuteriums at the α-chain (**2DH**), at the β-chain (**2HD**), and at both chains (**2DD**), respectively). To further study the reactivity of gas-phase peptide radical ions (**3**

versus **6**) with different hydrogen environments (*i.e.*, whether the system is “hydrogen-rich” or “hydrogen-deficient”), we prepared the model peptide systems depicted in **Scheme 3.1**. Acetylation of the model peptide AARAAACAA, followed by disulfide bond formation with the parent peptide, provides a structural mimic (**5**) of the regiospecific acetyl radical peptide cation (**3**) generated by FRIPS reagent conjugates (**1** or **2**). Electron capture by the triply protonated mimic (**5**) produces the charge-reduced doubly protonated ion (**6**). The two peptide cations **3** and **6** that are produced, respectively, by collisional activation of FRIPS conjugates and ECD, are differentiated by a localized radical center in the “hydrogen-deficient” species (**3**) vs. the presence of a labile hydrogen atom in the “hydrogen-rich” species (**6**). We show that activation of both species leads predominantly to cleavage of the disulfide linkage. Reaction mechanisms are proposed for each, showing that distinct reactivity in each model system results from the nature of the radical centers and structural features which constrain reaction energetics. Quantum chemical calculations using third generation meta-hybrid density functionals (BMK¹⁷⁶, M05-2X¹⁷⁷ and M06-2X¹³¹, chosen for their better performance in organic radical reactions) along with the conventional B3LYP^{128,129} functional were performed to quantify energetics of observed reaction processes.

3.2.Experimental

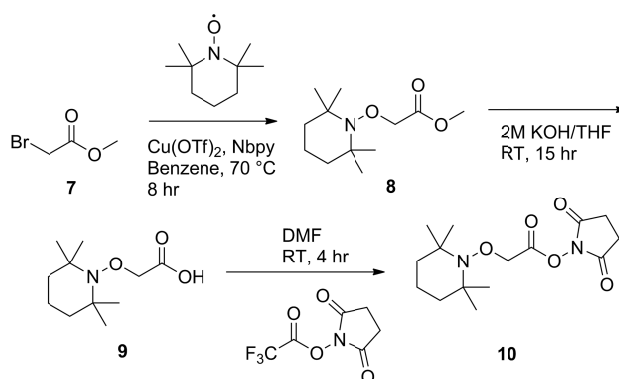
3.2.1. Peptide Fragmentation Nomenclature

Peptide fragmentation nomenclature used in this study for c- and z-type ions produced by ECD and ETD versus a- and x-type ions produced by FRIPS is explained in details in Supporting Information. Briefly, we follow the ECD type nomenclature described in the first ECD paper¹³ for both FRIPS and ECD fragment ions.

3.2.2. Materials

The model peptides, AARAAACAA, in 95% peptide purity, and AARAAACAA with a deuterated β -carbon at the cysteine residue, in 98% isotope purity, and 75% peptide purity, were purchased from Biomer Technology LLC (Pleasanton, CA, USA). Vasoactive intestinal peptide (VIP) from human, residue 1-12 (HSDAVFTDNYTR) that simulates tryptic peptides, and Arg8-Vasopressin (CYFQNCPRG-NH₂, Cys1 and Cys6 are connected via a disulfide bond) were purchased from AnaSpec (San Jose, CA, USA). Arg8-Conopressin G (CFIRNCPRG-NH₂, Cys1 and Cys6 are connected via a disulfide bond) was purchased from Bachem (Torrance, CA, USA). A soluble free-radical initiator, Vazo 68, was purchased from DuPont (Wilmington, DE, USA). Acetic anhydride was purchased from Mallinckrodt Inc. (Phillipsburg, NJ, USA). All solvents are HPLC grades and were purchased from EMD Merck (Gibbstown, NJ, USA). Sequencing grade TPCK treated trypsin was purchased from Promega (Madison, WI, USA). All other chemicals were purchased from Sigma-Aldrich (St. Louis, MO, USA) unless otherwise specified. For desalting, OMIX 100 μ L size C-18 tips were purchased from Varian Inc. (Palo Alto, CA, USA).

3.2.3. Synthesis of TEMPO-based FRIPS Reagent



Scheme 3.2

Synthesis strategy for the second generation TEMPO-based FRIPS reagent (**10**) is summarized in **Scheme 3.2**. The previous development by Lee *et al.*¹⁷⁵ was modified by replacing 2-(bromomethyl)benzoic acid methyl ester with methyl 2-bromoacetate for the current study. Briefly, TEMPO is coupled to the acetyl methyl ester group, followed by deprotection and activation of the carboxylic acid group. Ten mg/mL of the final product (**10**) in acetonitrile (ACN) was reacted with 50 μ g of model peptides in 100 mM phosphate buffer (pH 8.5) for 2 hr. After desalting, the resulting peptide conjugates were analyzed by electrospray ionization (ESI) ion trap mass spectrometers. See Supporting Information for details on the synthesis of the TEMPO-based FRIPS reagent and peptide conjugation.

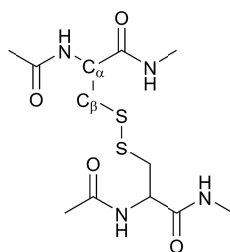
3.2.4. Mass Spectrometry

FRIPS experiments were performed using a LCQ Deca XP ion trap mass spectrometer (Thermo, San Jose, CA, USA). Prepared peptide solutions were directly infused to the mass spectrometer at 3 μ L/min by a syringe pump with an electrospray ionization source. Critical parameters of the mass spectrometer include spraying voltage 3.5 kV, capillary voltage 41~42 V, capillary temperature 275 °C and tube lens voltage -50~60 V. Other ion optic parameters were optimized by the auto-tune function in the LCQ tune program for maximizing the signal intensity. The precursor isolation window for MSⁿ experiments was set to 3.5 m/z and normalized collisional energy in the LCQ tune program was varied from 23% to 28% based on residual precursor ion intensities. For FRIPS and CID spectra, 100 scans were recorded.

ECD was performed in the Proteome Exploration Laboratory of the Beckman Institute at Caltech using a 7-tesla linear ion trap Fourier transform ion cyclotron resonance (LTQ-FTICR) mass spectrometer (Thermo, San Jose, CA, USA) equipped with the Nanomate (Advion BioSciences Inc., Ithaca, NY, USA) nanospray unit. The spraying voltage was 1.4 kV and the gas

pressure was 0.3 psi. Critical parameters of the mass spectrometer include capillary voltage 49 V, capillary temperature 200 °C and tube lens voltage 180 V. Other ion optic parameters were optimized by the auto-tune function in the LTQ tune program for maximizing the signal intensity. The target resolution at 400 m/z was set to 100,000. The precursor isolation window for ECD experiments was set to 5.0 m/z and electron irradiation occurred for 100ms at 5% of the full energy scale in the LTQ tune program, corresponding to electron energies less than approximately 1 eV. For ECD spectra, 100 scans were recorded. In particular, the TEMPO-based FRIPS reagent conjugates of intermolecular disulfide bond containing peptides (**2**), Arg8-Conopressin G, and trypsin digested Arg8-Conopressin G were analyzed by ion trap scans in a hybrid LTQ-FTICR mass spectrometer with the nanospray and ion optics conditions described above.

3.2.5. Quantum Chemical Calculation



N,N'-diacetyl-cystine-*N*-methylamide

Scheme 3.3

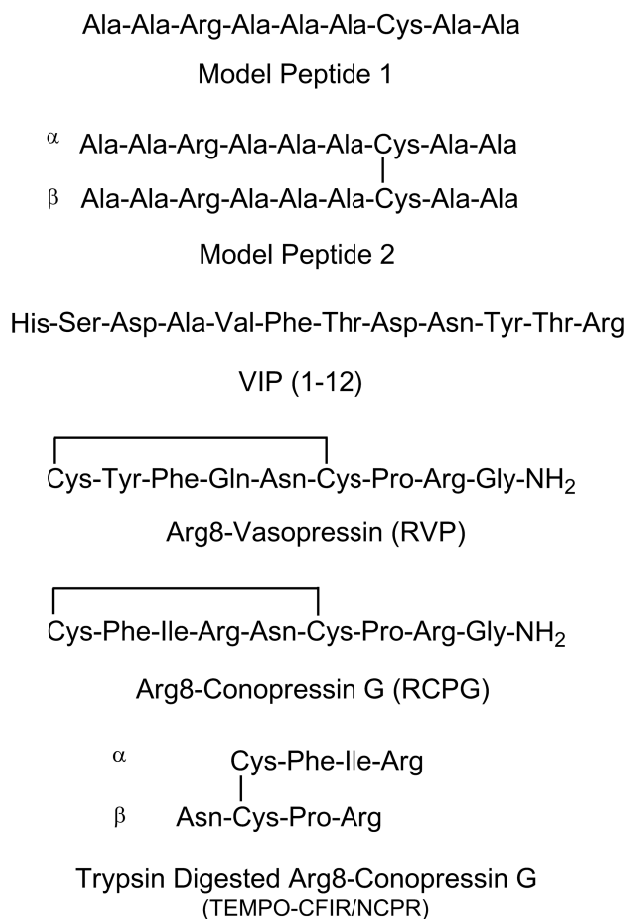
N,N'-diacetyl-cystine-*N*-methylamide (**Scheme 3.3**) was used for the simple model system to describe the intermolecular disulfide bond linked peptide used in this study, CH₃CONH-[AARAAACAA]-S-S-[AARAAACAA] (**5**). Initial geometries were generated by the MC/MM conformer search using Macromol 8.0 (Schrödinger Inc., Portland, OR, USA) as implemented in

Maestro 8.0 (Schrödinger Inc., Portland, OR, USA) under the Linux environment. The OPLS 2005 was used for the force field model. Within 5 kcal/mol energy, all low-energy conformers were initially recorded. After manual screening of obtained structures to avoid redundancy, low-energy conformers were selected for further structure optimization by density functional theory (DFT). For radical species, *ad hoc* assignment of the formal charge state was employed to implement MC/MM calculations for conformer searching. In particular, conformers of the C_β hydrogen abstracted *N,N'*-diacetyl-cystine-*N*-methylamide radical were searched by substitution of the β-carbon with boron to simulate the trigonal bonding environment. Each conformer was subject to a geometry optimization using Jaguar 7.5 (Schrödinger Inc., Portland, OR, USA) at the B3LYP/6-31G(d) level. By monitoring the occurrence of imaginary vibrational frequencies, only non-transition state structures (*i.e.*, no imaginary vibrational frequency) were further optimized using a higher basis set at the B3LYP/6-311++G(d,p) level. The transition state structures were searched using the LST or QST methods by interpolating initial guesses for reactants, products and transition states. Single point energy was refined using Q-Chem 3.1 (Q-Chem Inc., Pittsburg, PA, USA) by the BMK, M05-2X, M06-2X and B3LYP density functionals with the 6-311++G(3df,3pd) basis set. The three new generation meta-hybrid functionals other than B3LYP were chosen for their ability to more reliably predict the energetics of organic radical reactions.^{131,176} For the open-shell systems, the spin-unrestricted method was used. All calculations were performed using computational resources kindly provided by the Material and Process simulation center at the Beckman Institute, Caltech.

3.3.Results and Discussion

All peptides used in this study are shown in **Scheme 3.4**. The model peptide 1 and 2 are the simple cysteine and intermolecular disulfide bond containing peptides. The N-terminal amine of

the α -chain in the model peptide 2 is acetylated for ECD or conjugated by FRIPS reagents. The β -deuteriums are inserted in each peptide chain of the model peptide 2 to probe the mechanism of disulfide bond cleavage (See also **Scheme 3.1**). The VIP (1-12) peptide is used for the validation of sequencing performance of the newly prepared FRIPS reagent (**10**). This model system simulates FRIPS spectra of tryptic peptides which are produced by trypsin, the most popular protease in the MS-based bottom-up proteomics analysis. Arg8-Vasopressin and Arg8-Conopressin G are chosen to investigate the reactivity of the acetyl radical with the intramolecular disulfide bond in various charge states (*i.e.*, +1 for Arg8-Vasopressin and +2 for Arg8-Conopressin G). These two peptides share many structural features such as an intermolecular disulfide bond between Cys1 and Cys6, and the amidated C-terminal, which form the vasopressin family peptides and show similar bioactivities.¹⁷⁸ An intermolecular disulfide bond containing model peptide is produced by trypsin digestion of the TEMPO-based FRIPS reagent conjugate of the Arg8-Conopressin G (TEMPO-CFIR/NCPR). This model peptide is introduced to investigate the reactivity of the acetyl radical with an intermolecular disulfide bond when other amino acids having more reactive hydrogens of the α - and β -carbons than those of alanine are present.



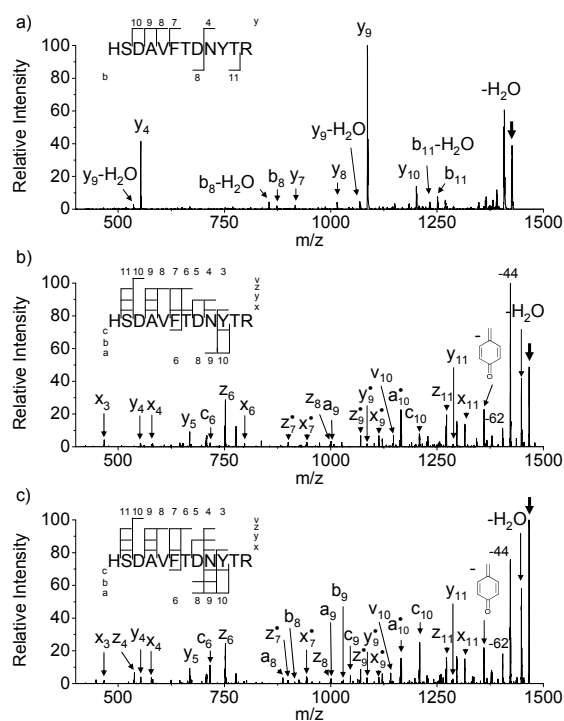
Scheme 3.4

3.3.1. VIP (1-12)

Evaluation of the second generation TEMPO-based FRIPS reagent is performed by singly protonated HSDAVFTDNYTR peptide cation (**Figure 3.1**). The CID spectrum of singly protonated VIP is dominated by y_4 and y_9 ions from the low-energy salt bridge cleavage pathway at the C-terminal sides of aspartic acids in the presence of the protonated arginine residue, yielding poor sequence coverage (**Figure 3.1a**, 6 out of 11, 55%).^{10,11} The FRIPS spectra of singly protonated VIP from Vazo 68 and TEMPO-based FRIPS reagents exhibit extensive

backbone cleavage fragments which cover almost the full sequence of the peptide (**Figures 3.1b** and **c**, 10 out of 11, 91%). Almost all ion types of backbone fragments such as a, b, c, v, x, y and z ions appear in both **Figures 3.1b** and **c**. Not unexpected, the spectra from the two different FRIPS reagent conjugates (**Figures 3.1b** and **c**) share many common ions and their intensities are nearly identical. Observed backbone fragments are produced by either H-atom abstraction from the β -carbons, followed by β -cleavage (a and x^{\bullet} ions, and z^{\bullet} ions by CONH loss from x^{\bullet} ions) or the charge-remote amide bond cleavage (b and y ions). H-atom transfer between a-type neutral fragment and x^{\bullet} ion after β -cleavage may produce even electron x ions. This phenomenon is more dominant for smaller fragment ions such as x_3 and x_4 . Interestingly, the formation of c_6/z_6 ions and a_{10}^{\bullet}/c_{10} ions at the N-terminal of the threonine residues (Thr7 and Thr11) that cannot be simply explained by H-atom abstraction from the β -carbons, followed by β -cleavage is observed (**Figures 1b** and **c**). The same types of fragment ions nearby the threonine or serine residues are also found in the previous studies.^{179,180} We are investigating the mechanism of this process and it will be independently reported. Initiation of side-chain loss usually occurs by H-atom abstraction from the α - or γ -carbons of backbone amino acids, followed by β -cleavage. Types of side-chain loss in hydrogen-deficient peptide radicals are thoroughly investigated by Sun *et al.*¹⁷⁹ Carbon dioxide loss (-44 Da) is induced by H-atom abstraction from the carboxyl groups at the aspartic/glutamic acid residues or the C-terminal carboxylic acid. Isobaric \bullet CONH₂ neutral loss produced by the H-atom abstraction from the α -carbon of asparagine, followed by β -cleavage may partially account for -44 Da loss in **Figures 1b** and **c**. Phenolic H-atom abstraction from tyrosine yields loss of para-quinone methide (-106 Da) via radical rearrangement of the phenoxy radical group (**Figures 1b** and **c**).

Figure 3.1 CID and FRIPS of singly protonated HSDAVFTDNYTR

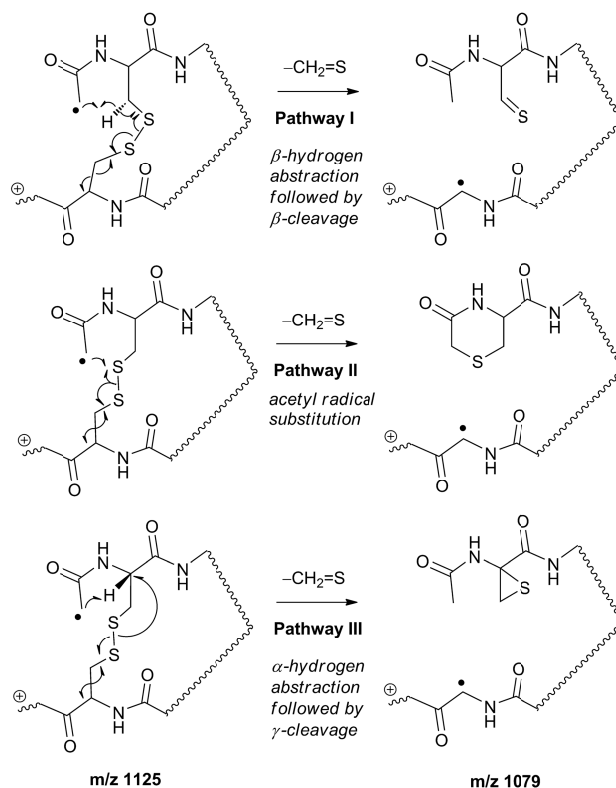


The CID spectrum (a) and FRIPS (Vazo 68 and the TEMPO-based reagent) spectra (b and c, respectively) of singly protonated HSDAVFTDNYTR. The CID spectrum (a) is dominated by y_4 and y_9 ions from the low-energy salt bridge cleavage pathway at the C-terminal sides of aspartic acids, effected by the protonated arginine residue. This results in poor sequence coverage (6 out of 11, 55%). b) and c) are nearly identical, yielding mainly backbone cleavage fragments (10 out of 11, 91% sequence coverage) and neutral losses. Bold arrows indicate the precursor ions.

3.3.2. Arg8-Vasopressin

Figures 3.2a-d depict FRIPS of Arg8-Vasopressin. The TEMPO-based FRIPS reagent (**10**) was conjugated to the N-terminal amine of Arg8-Vasopressin with a conversion yield of approximately 90% based on the relative signal intensities between FRIPS reagent conjugated and unmodified Arg8-Vasopressin peaks in **Figure 3.2a**. The singly protonated TEMPO-based FRIPS reagent conjugate of Arg8-Vasopressin (m/z 1281) is collisionally activated to generate the regiospecific acetyl radical cation (m/z 1125) by loss of TEMPO radical (**Figure 3.2b**). This process is energetically favored to produce the abundant acetyl radical cation. Thus it allows us to proceed to the following CID experiments up to MS4 for peptide sequencing by ensuring strong ion signals. It is less practical when Vazo 68 is used with the consequence that MS5 is required to characterize the intramolecular disulfide bond in Arg8-Vasopressin. Collisional activation of the acetyl radical cation (m/z 1125) induces mainly CH_2S loss (m/z 1079) by cleaving the S–S bond.

Figure 3.2. FRIPS and ECD of Arg8-Vasopressin. a) ESI-MS1 of the TEMPO-based FRIPS reagent conjugate of Arg8-Vasopressin. b) CID of the singly protonated TEMPO-based FRIPS reagent conjugate of Arg8-Vasopressin, m/z 1281 (MS2). c) CID of the acetyl radical cation, m/z 1125 (MS3). d) CID of the CH_2S loss product from the acetyl radical cation, m/z 1079 (MS3). RVP is Arg8-Vasopressin, C^{S} is thioaldehyde, thiomorpholin-3-one or thiirane products, and G^{\cdot} is glyceryl α -carbon radical. See **Scheme 3.5** for the proposed reaction mechanisms. e) ECD of the doubly protonated Arg8-Vasopressin. See **Scheme 3.6** for notations of $z_n\text{-S}$ ions. * denotes electronic noise peaks. Bold arrows indicate the precursor ions.



Scheme 3.5

We propose that this process is initiated by H-atom abstraction at the β -carbon of Cys1, followed by β -cleavage (**Scheme 3.5**, pathway I). The resulting radical cation at m/z 1079 contains a modified residue whose side chain is thioaldehyde ($-\text{CH}=\text{S}$) at Cys1 position (the 2-amino-3-thioxopropanoic acid residue) and the glyceryl α -carbon radical residue at Cys6 position. The possibility of H-atom abstraction at the β -carbon of Cys6 was considered but no correlated

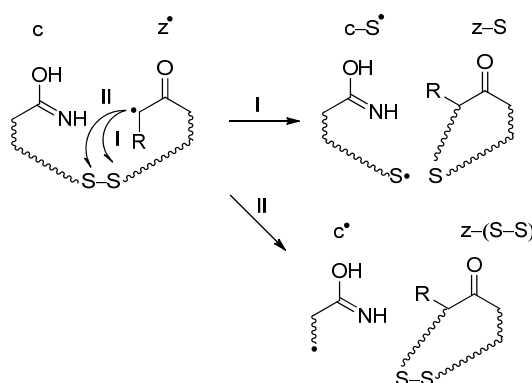
fragments were observed in CID of m/z 1079 (**Figure 3.2d**). Instead, the six-membered ring intermediate favors reaction at the β -carbon of Cys1. No direct β -cleavage from the glyceryl α -carbon radical residue (*e.g.*, b_6^*/y_4 and b_7/y_3^*) is observed. The glyceryl α -carbon radical cation at m/z 1079 is directly isolated from the MS2 stage and further collisionally activated in MS3 (**Figure 3.2d**). Following H-atom abstraction by the glyceryl radical at other α - and β -carbon sites, followed by β -cleavage leads to side-chain losses (17, 33, 58, and 71 Da) and backbone fragmentation (b, x, z, v and w ions, **Scheme 3.5**). From these product ions, the peptide sequence and the position of the intramolecular disulfide bond are assigned (**Figure 3.2d**). Compared to what we observed in the previous study of alkali and alkaline earth metal complexes of disulfide bond containing peptides³⁹, the sequence coverage after CH_2S loss is more extensive, including six out of eight possible backbone fragments (**Figure 3.2d**).

An alternative mechanism for CH_2S loss via dissociative addition of the acetyl radical, so called radical substitution ($\text{S}_{\text{H}2}$) reaction, to the disulfide bond is described in **Scheme 3.5**, pathway II.¹⁸¹ Radical substitution forms the stable six-membered thiomorpholin-3-one ring structure at the N-terminal, and releases the thiyl radical group by cleaving S–S bond at the counterpart cysteine residue. The residual internal energy after S–S bond cleavage leads to subsequent loss of CH_2S , yielding the glyceryl α -carbon radical group at Cys6.

H-abstraction at the α -carbon of Cys1, followed by γ -cleavage is also considered (**Scheme 3.5**, pathway III). The first step of this pathway, H-abstraction reaction at the α -carbon, is energetically favored over abstraction at the β -carbon (tertiary versus secondary hydrogens). Also, the final thiirane product is more stable than thioaldehyde, yielding a thermodynamically favored process. However, in general 1,4-H transfer is rarely observed¹⁸² and its steric hindrance over 1,5-H transfer makes this pathway kinetically less favored. Note that the overall fragmentation results in the pathway II and III after loss of CH_2S are indistinguishable by their mass to charge ratios to

those of the pathway I. In this regard, it is hard to discern the relative portions of each reaction pathway proposed in **Scheme 3.5**. We will later investigate this mechanism with intermolecular disulfide bond containing peptides that may experience less steric hindrance for H-abstraction at the α -carbon via the remote way, not by the direct 1,4 interaction.

ECD of the doubly protonated Arg8-Vasopressin is shown in **Figure 3.2e**. The most prominent process is loss of $\text{HS}\cdot$ that is involved with multiple bond cleavages in the disulfide bond. The same neutral loss was also observed in the previous study on the analogue model system, Lys8-Vasopressin.⁵³ Many $\text{N}-\text{C}_\alpha$ bonds are cleaved by ECD (6 out of 8, z_2 , w_4 , and z_{5-8}) and the observed sequence coverage is the same as FRIPS.



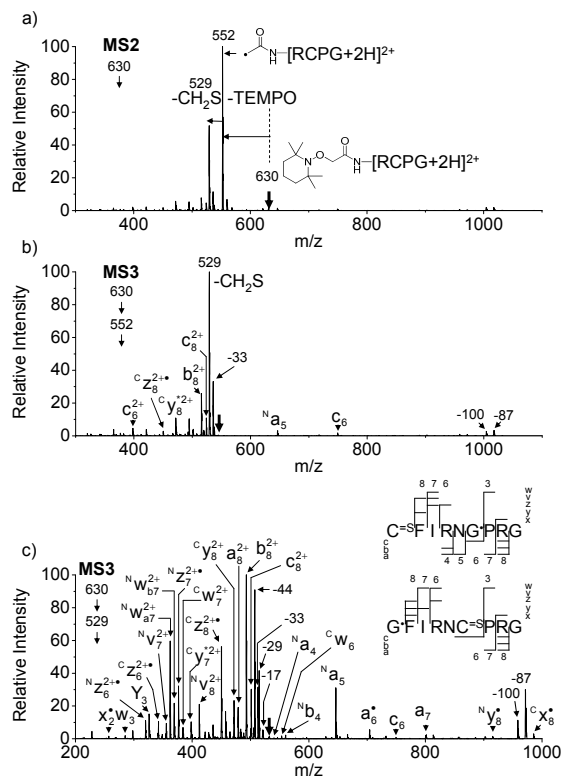
Scheme 3.6

One possible mechanism for intramolecular disulfide bond cleavage by ECD was previously proposed as follows.⁵³ The α -carbon radicals of the nascent z' ions generated by $\text{N}-\text{C}_\alpha$ bond cleavage may attack one of the sulfur atoms in the disulfide bond, followed by disulfide bond cleavages (**Scheme 3.6**, pathway I for S-S bond cleavage and pathway II for C-S bond cleavage). As a result, two covalent bonds that form a cyclic peptide structure are cleaved, releasing $z_n\text{-S}$ ions (**Figure 3.2e**). As an exception, the w_{a4} ion is formed via β -cleavage of the α -carbon radical

of the nascent z' ion by cleaving a C–S bond (**Figure 3.2e**). This previously suggested mechanism explains both N–C $_{\alpha}$ bond and intramolecular disulfide bond cleavages. In addition, regardless of the actual mechanism for the formation of the nascent z' ions (the Cornell versus the Utah-Washington), the final results after disulfide bond cleavage are identical.

H-atom transfer to one of the sulfur atoms, followed by disulfide bond cleavage by forming the thiyl radical ($-S\bullet$) and thiol groups ($-SH$) is also considered.^{53,171} The relatively high H-atom affinity of the disulfide bond makes this mechanism more plausible.^{53,171} This process can also explain the observed dominant process for disulfide bond cleavage compared to N–C $_{\alpha}$ bond cleavages. For example, the most abundant product from HS \bullet loss (**Figure 3.2e**) is associated with multiple bond cleavages, which is more easily explained by direct dissociative H-atom addition to the disulfide bond. The nascent thiyl radical can abstract H-atom from the α -carbon of the counterpart cysteine residue.^{183,184} The resulting α -carbon radical can undergo β -cleavage, yielding HS \bullet loss. Direct electron capture or intramolecular electron transfer to the Coulomb stabilized σ^* orbital of the S–S bond, followed by proton transfer yields the same thiyl radical and thiol products.⁷²

Figure 3.3 FRIPS of doubly protonated Arg8-Conopressin G



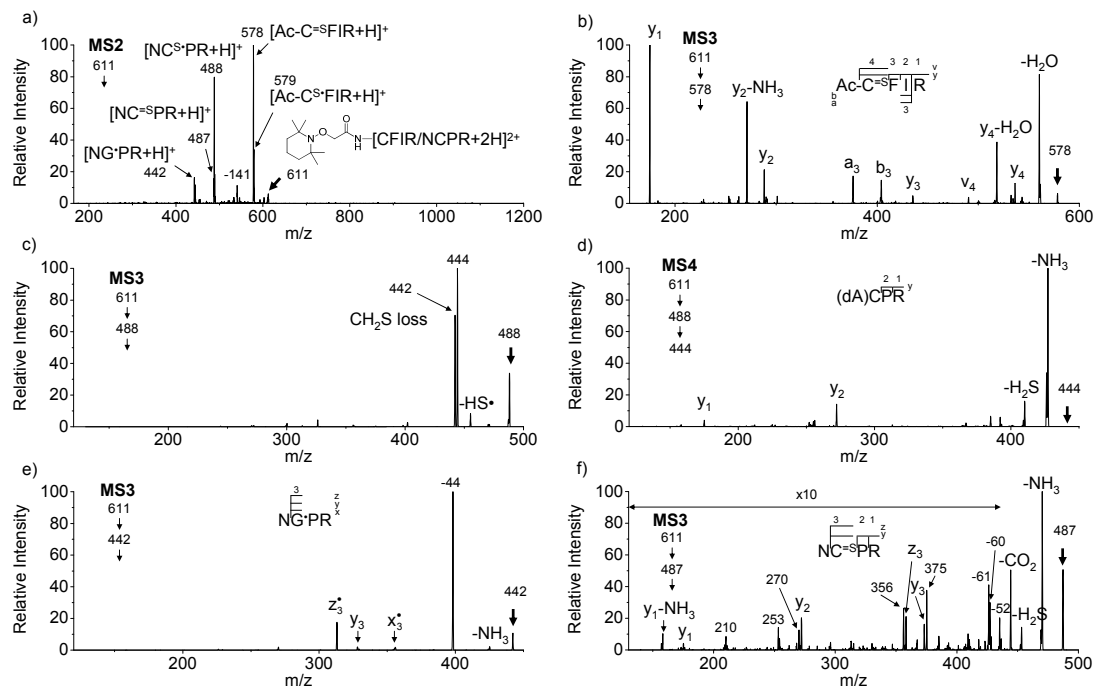
FRIPS of doubly protonated Arg8-Conopressin G. a) CID of doubly protonated TEMPO-based FRIPS conjugate of Arg8-Conopressin G at m/z 630 (MS2). b) CID of the acetyl radical containing Arg8-Conopressin G dication at m/z 552 (MS3). c) CID of the CH_2S loss dication from the acetyl radical dication at m/z 529 (MS3). RCPG is Arg8-Conopressin G, C^{S} is thioaldehyde, thiomorpholin-3-one or thirane products, and G^{\cdot} is glyceryl α -carbon radical. Superscripts (“N” and “C”) on the left side of the fragment ions indicate the position of the C^{S} residue that is located at the N-terminal or the C-terminal of the peptide. * denotes ammonia loss. Bold arrows indicate the precursor ions.

3.3.3. Arg8-Conopressin G

FRIPS spectra of doubly protonated Arg8-Conopressin G are shown in **Figure 3.3**. Compared to the FRIPS results for singly protonated Arg8-Vasopressin (**Figure 3.2**), we investigate the effect of the charge state of the precursor ion on the FRIPS fragmentation pathways (*i.e.*, disulfide bond, backbone and side-chain) with two protonated arginine residues. The regiospecific acetyl radical dication (m/z 552) is formed by collisional activation of the TEMPO-based FRIPS reagent conjugate of Arg8-Conopressin G dication (m/z 630, **Figure 3.3a**). Collisional activation of the acetyl radical dication (m/z 552) mainly produces the disulfide bond cleavage product (m/z 529) via CH_2S loss (**Scheme 3.5**). Concomitant losses of TEMPO radical and CH_2S occur regardless of the charge state (+1 or +2) of the precursor ions in both our model intramolecular disulfide bond containing peptides (**Figures 3.2** and **3.3**). The prominent CH_2S loss is also observed in the MS2 stage (**Figure 3.3a**), which allows us to perform peptide sequencing in the MS3 stage with improved ion signals by reducing one step of collisional activation (**Figure 3.3c**). Interestingly, compared to the FRIPS spectrum of singly protonated Arg8-Vasopressin (**Figure 3.2d**), the FRIPS spectrum of doubly protonated Arg8-Conopressin G is the mixture of fragments of two possible glycy radical dications produced by loss of CH_2S at each cysteine residue. This indicates that the gas-phase conformation of doubly protonated Arg8-Conopressin is more flexible, allowing the acetyl radical group to react with both Cys1 and Cys6 residues. Although the peptide sequence of Arg8-Conopressin G is very similar to Arg8-Vasopressin, it is believed that the additional protonated arginine residue within the region bounded by the disulfide bond dramatically modifies its gas-phase structure, showing the distinct fragmentation pattern by forming two possible glycy radical dications. As a result, the observed fragment ions from collisional activation of CH_2S loss dication (m/z 529) are attributed to two possible glycy radicals at Cys1

and Cys6 positions, respectively (**Figure 3.3c**, *i.e.*, ${}^N Z_6^{2+\bullet}$ versus ${}^C Z_6^{2+\bullet}$ where the upper-left N or C indicate the positions of the resulting even electron species at the original cysteine residues after disulfide bond cleavage). The overall sequence coverage is extensive, revealing the full amino acid sequence of Arg8-Conopressin G (**Figure 3.3c**, 8 out of 8).

The reactivity of the intermolecular disulfide bond is investigated by collisional activation of doubly protonated TEMPO-CFIR/NCPR (a tryptic digest of the TEMPO-conjugated Arg8-Conopressin G, **Figure 3.4**). This model system simulates tryptic digests of disulfide bond containing proteins where cleavage fragments in part comprise two peptide chains derived from the original protein backbone, held by an intermolecular disulfide bond. Collisional activation of doubly protonated TEMPO-CFIR/NCPR mainly produces products from S–S bond cleavage. Interestingly, the product from TEMPO loss (–156 Da) is not observed (**Figure 3.4a**). Rather, loss of 141 Da (2,2,6,6-tetramethylpiperidine) is observed at m/z 540.8, indicating N–O bond cleavage (**Figure 3.4a**). This product may result from proton transfer from the protonated arginine residue to the TEMPO nitroxide tertiary amine residue and subsequent rearrangement for bond cleavage.

Figure 3.4 FRIPS of doubly protonated TEMPO-CFIR/NCPR

FRIPS of doubly protonated TEMPO-CFIR/NCPR. a) CID of doubly protonated TEMPO-CFIR/NCPR at m/z 611 (MS2). Highly selective S–S bond cleavage is observed, yielding both α - and β - chain cations. b) CID of the α -chain, Ac-C^SFIR cation (even electron species) at m/z 578 (MS3), yielding the sequence of the α -chain. c) CID of the β -chain, NC^SPR cation (odd electron species) at m/z 488 (MS3). Losses of 44 (\bullet -CONH₂, m/z 444) and 46 (CH₂S, m/z 442) Da are prominent. d) CID of the β -chain cation at m/z 444 (even electron species, MS4). e) CID of the β -chain cation at m/z 442 (odd electron species, MS3). f) CID of the β -chain cation at m/z 487 (even electron species, MS3). The CID spectra of various β -chain peptide cation (**Figures 5d, e, and f**) allow sequencing of the β -chain. See Supporting Information for the precursor ion structure, TEMPO-CFIR/NCPR. C^S is thioaldehyde, thiomorpholin-3-one or thiirane products, C^S is thiyl cysteine radical, G[•] is glycyl α -carbon radical, and “Ac-” is the acetylated N-terminal group except for the N-terminal thiomorpholin-3-one product case. Bold arrows indicate the precursor ions.

The resulting products from S–S bond cleavage have the thiyl radical and the counterpart even electron species, thioaldehyde, thiomorpholin-3-one or thiirane products (**Scheme 3.5**), respectively (**Figure 3.4a**). Subsequent losses of CH₂S or •CONH₂ from the thiyl radical at m/z 488 by CID yield the glycyll α-carbon radical (m/z 442) at Cys2 and dehydroalanine (m/z 444) at Asn1, respectively (**Figures 3.4a and c**). Collisional activation of the observed products in **Figure 3.4a** (m/z 578 of the α-chain, and m/z 442, 444, and 487 of the β-chain, respectively) provides *complete* sequence information of each peptide chain (**Figures 3.4b, d, e and f**). Even electron species such as cations at m/z 578 and 487 are mostly fragmented at amide bonds, yielding mainly b- and y-type ions with several neutral losses (**Figures 3.4b, d and f**). The glycyll α-carbon radical at m/z 442 abstracts H-atom from the β-carbon of the asparagine residue, which induces the C_α–C bond cleavage, releasing the x₃[•] ion. Concomitant loss of isocyanic acid (O=C=NH) from the x₃[•] ion yields the more stable z₃[•] ion (**Figure 3.4e**).

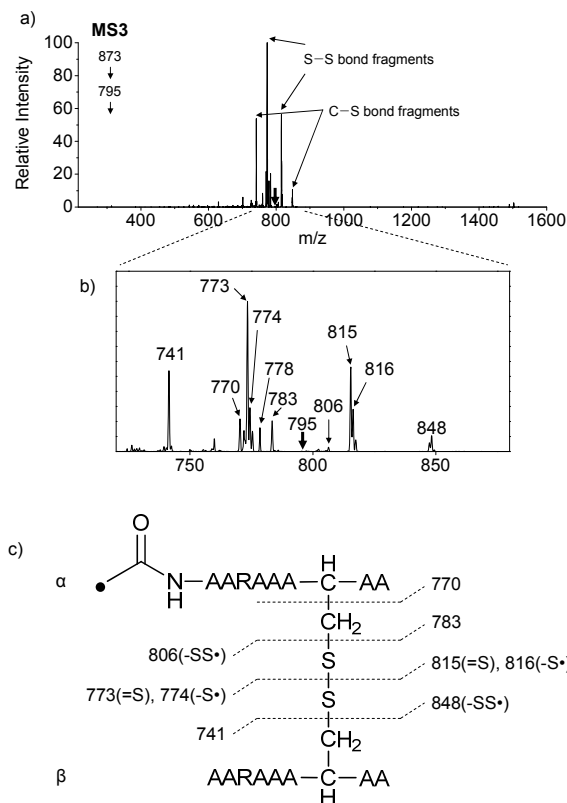
3.3.4. AARAAACAA Dimer

Figure 3.5 demonstrates disulfide bond cleavages effected by the acetyl radical in the model system, **3**. The regioselective acetyl radical group is generated by collisional activation of the doubly protonated TEMPO-based FRIPS reagent derivatized AARAAACAA peptide dimer (**2HH**, m/z 873). Further collisional activation of dication **3HH** severs the disulfide linkage, yielding various C–S (m/z 741, 783, 806, and 848) and S–S (m/z 773, 774, 815, and 816) bond cleavage fragments from each chain (**Figure 3.5b and c**). Compared to the FRIPS spectrum of doubly protonated TEMPO-CFIR/NCPR in **Figure 3.4**, abundant C–S bond cleavage fragments are observed in **Figure 3.5**. The difference should be noted that the acetyl radical dication at m/z 795 is subject to collisional activation in the MS3 stage (**Figure 3.5**), whereas the intact TEMPO conjugate is collisionally activated in the MS2 stage, yielding mainly the products from S–S bond

cleavage (**Figure 3.4**). Essentially no backbone fragmentation is observed due to higher bond dissociation energy of the C_β-H bond in alanine residues (**Figure 3.5a**).¹⁷⁹ In addition, S-S bond cleavage is more favored relative to C-S bond cleavage (**Table 3.1**). Relative fragmentation abundances are summarized in **Table 3.1**.

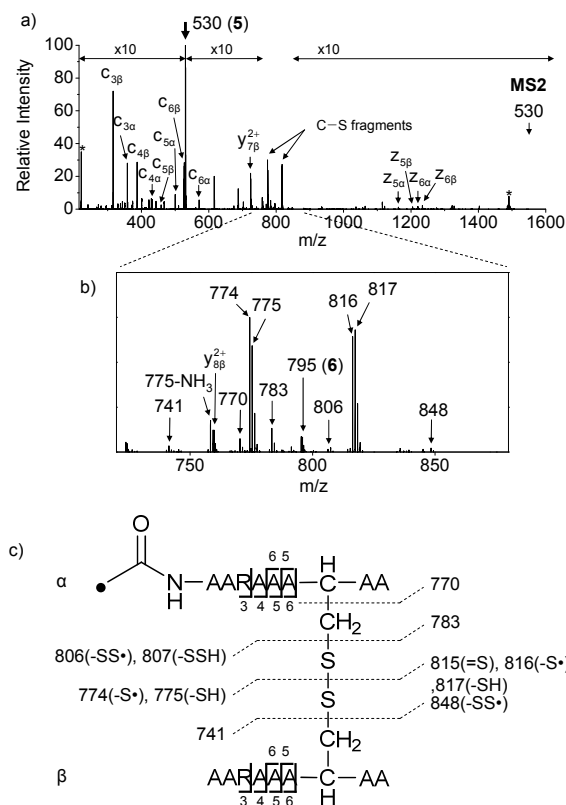
ECD of the triply charged intermolecular disulfide containing model peptide (**5**) is performed for comparison of the reactivity of the nascent charge-reduced radical dication to that of the regiospecific acetyl radical dication generated by FRIPS (**Figure 3.6**). The charge-reduced model peptide radical dication (**6**) produced by electron capture undergoes both backbone and disulfide fragmentations (**Figure 3.6a**). As noted in the introduction, disulfide bond cleavage is one of the most dominant reaction pathways in ECD and the process has been interpreted according to the viewpoints of both the Cornell⁵³ and Utah-Washington⁷² mechanisms. More specifically, even compared to FRIPS of **2HH**, ECD is dominated by S-S bond cleavage, in preference to other C-S bonds, and backbone fragmentations leading to c- and z-type ions (**Figure 3.6, Table 3.1**).

Figure 3.5 FRIPS of the doubly protonated AARAAACAA disulfide-bridged dimer



a) FRIPS of the doubly protonated AARAAACAA disulfide-bridged dimer (**3HH**, m/z 795). $\bullet\text{CH}_2\text{-CONH-[AARAAACAA]-S-S-[AARAAACAA]}$ (**3HH**, m/z 795, bold arrow) is generated by collisional activation of $\text{TEMPO-CH}_2\text{-CONH-[AARAAACAA]-S-S-[AARAAACAA]}$ (**2HH**, m/z 873) via loss of TEMPO radical. Essentially no backbone fragmentation is observed. b) Expansion of the m/z range in which disulfide cleavages occur. c) Scheme showing cleavage sites and fragment m/z values from each chain.

Figure 3.6 ECD of the triply charged alpha chain acetylated AARAAACAA disulfide-bridged dimer

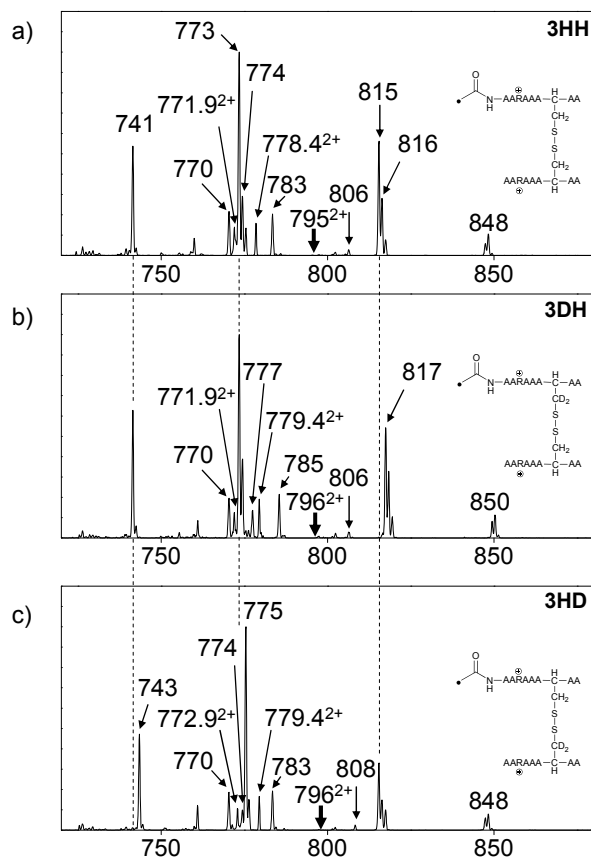


a) ECD of the triply charged alpha chain acetylated AARAAACAA disulfide-bridged dimer (**5**, m/z 530, bold arrow). The charge reduced doubly charged Ac-[AARAAACAA]-S-S-[AARAAACAA] (**6**, m/z 795) is generated by electron capture. Several ECD backbone fragments (c and z ions) are observed. b) Expansion of the m/z range in which disulfide cleavages occur. c) Scheme showing cleavage sites and fragment m/z values from each chain.

Table 3.1 Fragment Ions from FRIPS and ECD of AARAAACAA Disulfide-Bridged Dimer and Their Relative Yields.

FRIPS		ECD	
Fragment Type	Relative Yield (%)	Fragment Type	Relative Yield (%)
Backbone	0.5	Backbone	15.7
$a_{3\alpha}$, $a_{4\alpha}$, $a_{5\alpha}$, $a_{3\beta}$		$c_{3\alpha}$, $c_{3\beta}$, $c_{4\alpha}$, $c_{4\beta}$, $c_{5\alpha}$, $c_{5\beta}$, $c_{6\alpha}$, $c_{6\beta}$, $y_{6\beta}^{2+}$, $y_{7\beta}^{2+}$, $z_{5\alpha}$, $z_{5\beta}$, $z_{6\alpha}$, $z_{6\beta}$	
Side chain loss	1.2	Side chain loss	0
-101 and -89 from Arg			
Disulfide	98.3	Disulfide	84.3
C-S bond cleavage	27.1	C-S bond cleavage	8.3
m/z 741, 783, 806, 848		m/z 741, 783, 806, 807, 848	
S-S bond cleavage	72.9	S-S bond cleavage	91.7
m/z 770, 773, 774, 815, 816		m/z 758, 770, 774, 775, 815, 816, 817	

Figure 3.7 FRIPS of the deuterium-labeled doubly protonated AARAAACAA disulfide-bridged dimers



FRIPS of **3HH**, **3DH**, and **3HD**, (a, b, and c) respectively. Highly selective C-S (m/z 741/743, 783/785, 806/808, and 848/850) and S-S cleavage (m/z 773/775, 774/776, 815/817, 816/818) products are observed. See **Figure 3.5a** for the structures of the products. Almost no backbone fragmentation is observed, thus only the disulfide cleavage region is shown in here. Following CH_2S or CD_2S losses from the thiyl radicals at m/z 816 (a-3HH and c-3HD) or 818 (b-3DH) yield the glyceryl α -carbon radical product at m/z 770. No significant change is observed in their relative abundances of the products by S-S bond cleavage ($[\text{m/z } 817 \text{ in } \mathbf{3DH}] / [\text{m/z } 815 \text{ in } \mathbf{3HH}] = 0.995$, $[\text{m/z } 775 \text{ in } \mathbf{3HD}] / [\text{m/z } 773 \text{ in } \mathbf{3HH}] = \sim 1$) among FRIPS of **3HH**, **3DH**, and **3HD**. The results support pathway III, **Scheme 3.5**.

3.3.5. Deuterium-Labeled AARAAACAA Dimer

To probe the mechanisms of disulfide bond cleavage in the model system, we introduced β -deuteriums at disulfide bonds of the α - and β -chains in the model peptides (See **Scheme 3.1**. **3HH**, **3DH**, **3HD**, and **3DD**, respectively) for FRIPS experiments. **Figure 3.7** shows the FRIPS spectra of **3HH**, **3DH** and **3HD**, respectively. For C–S bond cleavage, H-abstraction at the α -carbon, followed by β -cleavage may occur, yielding the products at m/z 741/743, 783/785, 806/808 and 848/850, respectively. Comparison of peak intensities indicates the difference of an isotopic effect on product distributions. For S–S bond cleavage, if the mechanism is involved with H-abstraction at the β -carbons, significant isotope effects on the fragmentation pattern should be observed from these experiments. Surprisingly, in FRIPS of **3DH**, no significant change is observed in the relative abundances of the products involving S–S bond cleavage ($[m/z$ 817 in **3DH**] / $[m/z$ 815 in **3HH**] = 0.995, **Figure 3.7**).¹⁸⁵ Moreover, in the FRIPS spectrum of **3HD**, corresponding peaks possibly from pathway I in **Scheme 3.5** (H-abstraction at the β -carbon in the β -chain, followed by β -cleavage) are missing (m/z 817) or very small (m/z 774). Rather, the products at m/z 775 and 816 are observed in FRIPS of **3HD**, and their relative intensities appear to be very similar to those in **3HH** ($[m/z$ 775 in **3HD**] / $[m/z$ 773 in **3HH**] = ~ 1). This major discrepancy arising from peak analysis based on the pathway I or II in **Scheme 3.5** can be resolved by the proposed pathway III in **Scheme 3.5**. First of all, the initial H-abstraction at the α -carbon is not affected by deuterium substitution at the β -carbons. Also, the final products, thiirane and thiyl radicals, can explain the observed peaks, m/z 775 and 816, in FRIPS of **3HD** by having both deuteriums in each peptide chain without abstraction. Therefore, it is proposed that the major process for S–S bond cleavage is initiated by H-abstraction at the α -carbon, followed by γ -cleavage, yielding thiirane and thiyl radical.

The doubly protonated products generated by neutral losses from the acetyl radical dication precursor provide clues for the action of pathway II (direct acetyl radical substitution, **Scheme 3.5**). The doubly protonated product via CH_2S loss is observed at m/z 778. If the acetyl radical is substituted to the sulfur atom in the β -chain side to cleave the S–S bond, the resulting product is an intact linear dication. Namely, a covalent bond is formed between the N-terminal acetyl carbon and the sulfur in the β -chain, and the thiyl radical in the α -chain. Subsequent loss of CH_2S yields the glyceryl α -carbon radical as a doubly protonated species (for **3HH** at m/z 771.9 and for **3HD** at m/z 772.9). For FRIPS of **3DH**, loss of CD_2S is observed at m/z 771.9, confirming the proposed mechanism. The S–S bond cleavage product at m/z 815 in FRIPS of **3HD** via the acetyl radical substitution to the sulfur atom in the α -chain side, forming a cyclic structure between the N-terminal acetyl carbon and the sulfur in the α -chain, has the same mass to charge ratio as that from H-abstraction at the α -carbon, followed by γ -cleavage (pathway III in **Scheme 3.5**), which makes us hard to measure the contribution portion of the direct radical substitution mechanism. However, it is clear that the contribution of the direct radical substitution, which forms an intact dication when substituted to the sulfur atom in the β -chain, is not significant for S–S bond cleavage having no explanation for the base peak at m/z 775 in FRIPS of **3HD**. It can only be understood by pathway III in **Scheme 3.5**.

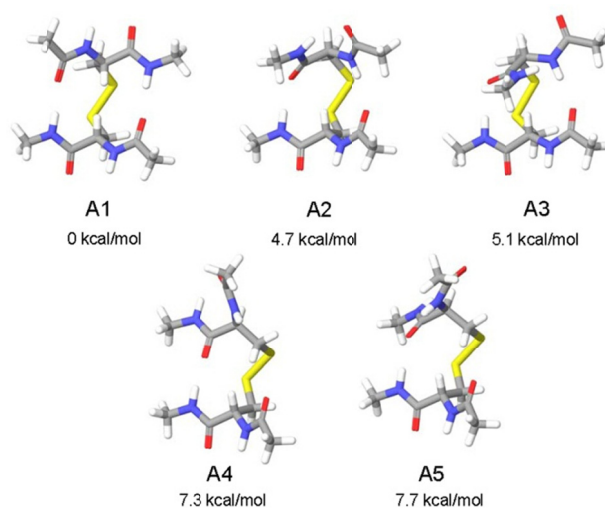
Based on the facts that the relative abundances of disulfide bond cleavage products show the similar distributions among FRIPS of **3HH**, **3DH**, and **3HD**, it is clear that pathway III (H-abstraction at the α -carbon, followed by γ -cleavage) is the dominant process for S–S bond cleavage, with a minor contribution from pathway II (direct radical substitution). The pathway I (H-abstraction at the β -carbon, followed by β -cleavage) may also play a role but only in a very minor way; the small product at m/z 774 in FRIPS of **3HD** is only explained by deuterium

abstraction (**Figure 3.7c**). For C–S bond cleavage, H-abstraction at the α -carbon, followed by β -cleavage may occur.

3.3.6. Quantum Chemical Computations

To investigate the energetics of the observed disulfide cleavage processes in collisionally activated acetyl radical cations, we use *N,N'*-diacetyl-cystine-*N*-methylamide (**Scheme 3.3**), and the untethered *N*-methylacetamide radical ($\bullet\text{CH}_2\text{-CONH-CH}_3$) as a model system. Several low-energy conformers of this model system are shown in **Figure 3.8**. The most stable conformer, **A1** is the all-trans form for amide bonds and hydrogen bonds are formed between amide oxygens and *N*-hydrogens in each chain. Other conformers have different dihedral angles from all-trans conformations between amide bonds, which distort hydrogen bonds between amide oxygens and *N*-hydrogens, yielding higher-energy conformers. Thus it is believed that the relative enthalpy difference in each conformer mainly results from disruption of interchain hydrogen bonds between amide *N*-hydrogens and carbonyl groups. Due to conformational diversity in the model system, we limit our consideration of reaction energetics to the lowest-energy structure in each reaction process without considering other possible conformers.

Figure 3.8 Low-energy conformers of model compounds



Low-energy conformers of *N,N'*-diacetyl-cystine-*N*-methylamide in relative enthalpy at 298.15K and 1 atm. Geometry optimization and thermochemical calculation were performed using B3LYP/6-311++G(d,p) level of theory and single point energy refinement was performed using B3LYP/6-311++G(3df,3pd) level of theory (in short, B3LYP/6-311++G(3df,3pd)// B3LYP/6-311++G(d,p)).

We first investigate C–S and S–S bond cleavages via abstraction of hydrogen atoms from α - and β -carbons, followed by β -^{15,175} and γ -cleavages, respectively. Relative enthalpy changes associated with each reaction channel are shown in **Figure 3.9**.

For both C–S and S–S bond cleavage reactions, the enthalpy changes predicted by B3LYP systematically deviate from the results estimated by other functionals by ~ 8 -10 kcal/mol (**Figure 3.9a**). This systematic deviation by B3LYP in the energetics of organic radical reactions has been reported previously.^{176,186,187} The better performances of BMK and M05/06-2X functionals have been demonstrated in comparison with G3(MP2)-RAD results.^{176,186,187} Therefore, we will discuss the energetics from the other three functionals, which are all in reasonable agreement.

As seen in **Figure 3.9**, H-abstraction at the β -carbon is exothermic but is a slightly less favored reaction (~ 4 kcal/mol) than H-abstraction at the α -carbon. Barriers for H-abstraction at each carbon are quite similar (~ 11 -15 kcal/mol). Following β -cleavage reaction for C–S bond cleavage is ~ 7 -10 kcal/mol endothermic, yielding acetyl-*N*-methyl dehydroalanine and acetyl-*N*-methyl cysteinyl radical and its barrier is ~ 14 -17 kcal/mol. The overall enthalpy change for C–S bond cleavage is only ~ 0 -2 kcal/mol endothermic. H-abstraction at the β -carbon, followed by S–S bond cleavage is endothermic by ~ 22 kcal/mol than that of H-abstraction at the α -carbon and subsequent C–S bond cleavage. In the S–S bond cleavage pathway via H-abstraction at the α -carbon, followed by γ -cleavage, the overall enthalpy change is ~ 2 -4 kcal/mol favored over H-abstraction at the β -carbon, followed by S–S bond cleavage. In this regard, it is shown that the energetic of thiirane formation is more favored than that of thioaldehyde. During the step of S–S bond cleavage via H-abstraction at the β -carbon, followed by β -cleavage, no barrier was found, forming a Van der Waals complex between thioaldehyde and thyl radical. For the dissociation of a Van der Waals complex, a certain barrier needs to be overcome by breaking two hydrogen bonds between amide bonds.

Figure 3.9 Reaction energetics of disulfide bond cleavages

a) Reaction energetics for S–S bond cleavage (left side) and C–S bond cleavage (right side) of *N,N'*-diacetyl-cystine-*N*-methylamide via hydrogen abstraction from α - and β -carbons, followed by β - and γ -cleavages showing relative enthalpies in kcal/mol. Geometry optimization and thermochemical calculation (298.15K and 1 atm) were performed using B3LYP/6-311++G(d,p) level of theory and single point energy refinement was performed using B3LYP (black), BMK (red), M05-2X (blue), and M06-2X (green) density functionals with the 6-311++G(3df,3pd) basis set, respectively. Some barrier heights are not known. *N*-methylacetamide radical ($\bullet\text{CH}_2\text{-CONH-CH}_3$) and *N*-methylacetamide are omitted in molecular structure drawings except for transition states of the α - and β -hydrogen abstraction but their enthalpies are included in the relative enthalpy diagram. b) Schematic drawing of reaction mechanisms for S–S bond cleavage (down side) and C–S bond cleavage (upper side) of *N,N'*-diacetyl-cystine-*N*-methylamide via hydrogen abstraction from α - and β -carbons, followed by β - and γ -cleavages.

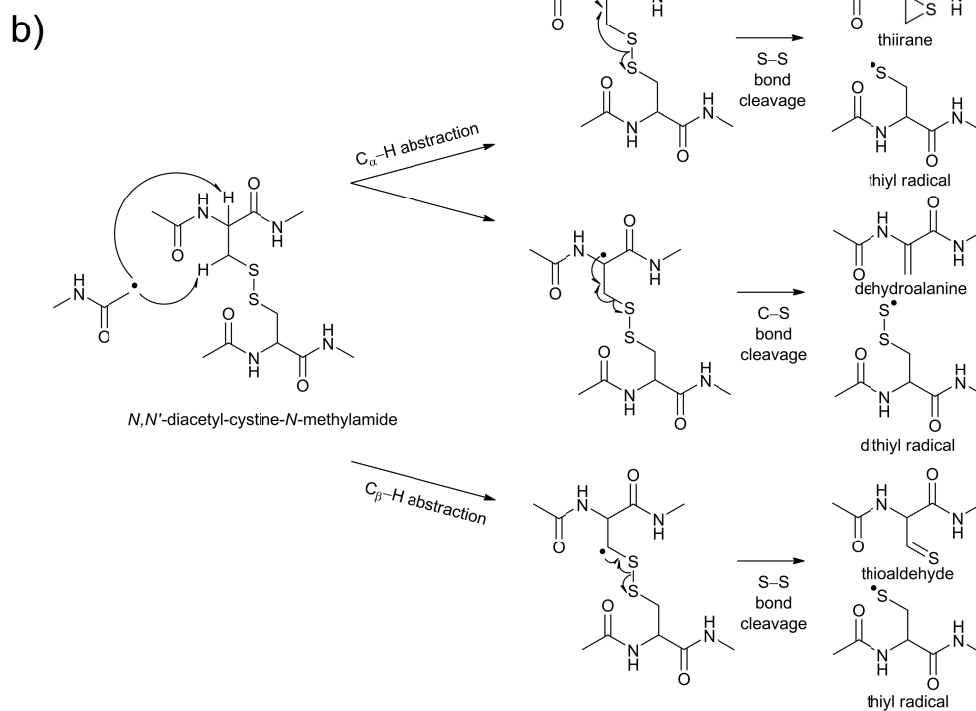
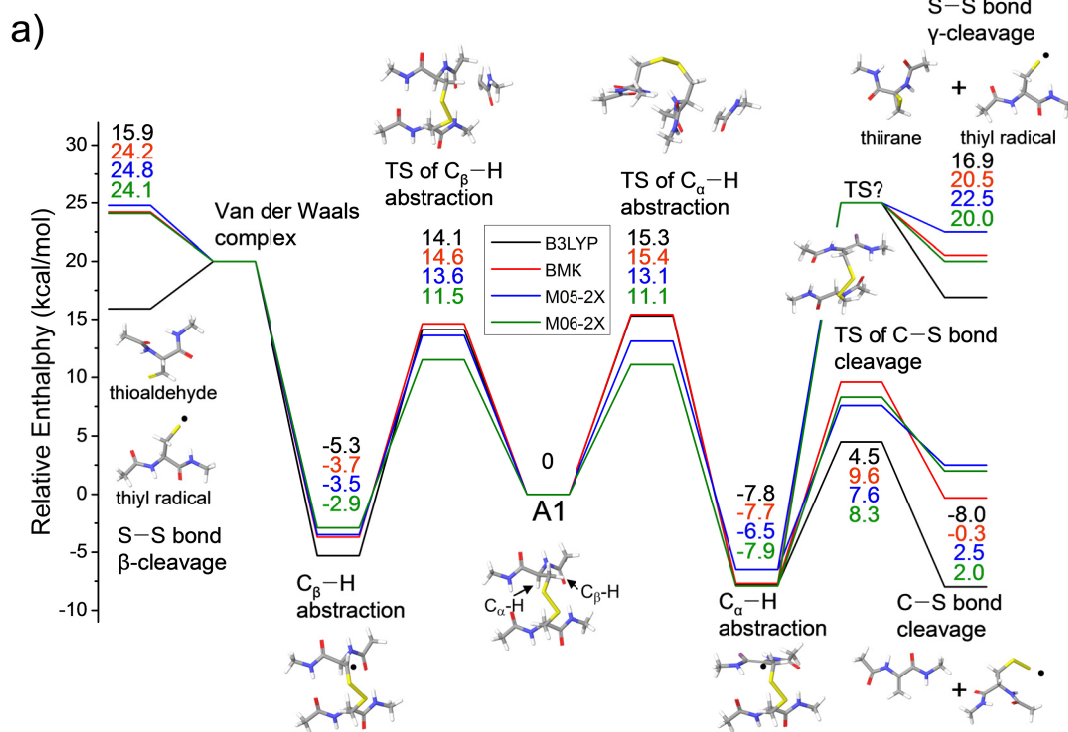
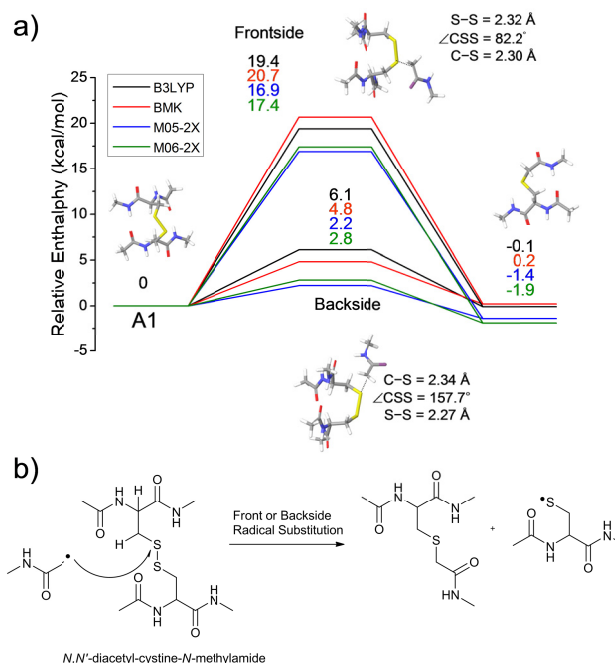


Figure 3.10 Reaction energetics of S–S bond cleavage by direct radical substitution



a) Reaction energetics for S–S bond cleavage of *N,N'*-diacetyl-cystine-*N*-methylamide by direct radical substitution via front- or backside, showing relative enthalpies in kcal/mol. Geometry optimization and thermochemical calculation (298.15K and 1 atm) were performed using B3LYP/6-311++G(d,p) level of theory and single point energy refinement was performed using B3LYP (black), BMK (red), M05-2X (blue), and M06-2X (green) density functionals with the 6-311++G(3df,3pd) basis set, respectively. b) Schematic drawing of reaction mechanisms for direct radical substitution.

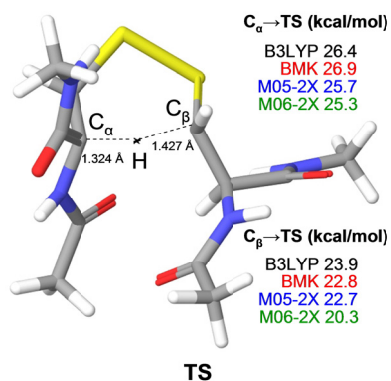
In addition, the energetics of the direct acetyl radical substitution to the sulfur atom, followed by S–S bond cleavage is considered (**Figure 3.10**). Formerly, the methyl radical substitution to dimetyldifulfide was studied using DFT.¹⁸¹ Two distinctive transition states were reported via front- and backside attack of the methyl radical and this process turns out to be concerted. The good orbital overlap via the backside attack between the σ^* orbital of S–S bond and the singly occupied molecular orbital (SOMO) of the methyl radical lowers the barrier for S–S bond cleavage. For our case, the formation of the hypervalent sulfur radical by substitution of the acetyl radical group is investigated whether the process is concerted or consecutive. However, intermediate structures having no imaginary vibrational frequency (*i.e.*, non-transient state structures) for the hypervalent sulfur radical were not found. Therefore, concomitant addition and dissociation of a S–S bond by addition of the acetyl radical are assumed (a concerted reaction pathway) and their energetics are evaluated. Enthalpy changes for S–S bond cleavage via direct addition of the acetyl radical group are estimated to be -0.1 , 0.2 , -1.4 and -1.9 kcal/mol by the B3LYP, BMK, M05-2X and M06-2X/6-311++G(3df,3pd)//B3LYP/6-311++G(d,p) levels of theories, respectively. This process is a lot more favored ($\Delta H = \sim 0$ kcal/mol) than what is observed in the β -hydrogen abstraction initiated process ($\Delta H = \sim 24$ kcal/mol). Also, the barrier for the backside attack (~ 2 - 5 kcal/mol) is substantially lower than all other reaction pathways. However, it should be noted that the alignment of reactant residues, the acetyl radical and the disulfide bond, is of particular importance for the radical substitution reaction. The reaction barrier is a very sensitive on the incident angle of the incoming acetyl radical (frontside versus backside, **Figure 3.10a**). The conformational space of the gaseous peptide ion may also not be highly populated for the successful orbital overlap between the σ^* orbital of S–S bond and SOMO of the acetyl radical lowers the barrier for S–S bond cleavage. Thus the very small ranges of incident angles may play an important role for the reaction in actual model peptides. In this

regard, it is concluded that the contribution of the direct radical substitution pathway is estimated to be rather low for S–S bond cleavage.

The H-atom migration between α - and β -carbons via the six-membered ring transition state is also investigated. H-atom abstraction from sterically more accessible β -carbons would favorably occur by the N-terminal acetyl radical group. If the barrier for the H-atom migration between α - and β -carbons is reasonably lower, the resulting radicals can initiate various C–S or S–S bond cleavages (**Figure 3.10**).

Figure 3.11 depicts the structure of the transition state for radical migration in which the transferred H-atom is approximately centered between the α - and β -carbons. The calculated reaction barrier from the β -carbon is rather high, ~ 20 - 23 kcal/mol but it is still 4-7 kcal/mol lower than the overall endothermicity of S–S bond cleavage of the β -carbon radical. Therefore, it is energetically reasonable for the H-atom migration to occur from the β -carbon to the α -carbon of a disulfide bond and the resulting α -carbon radical can undergo further C–S or S–S bond cleavages.

Figure 3.11 Transition state structure of hydrogen migration between α - and β -carbons



The optimized transition state structure of hydrogen migration between α - and β -carbons and reaction barriers from each side showing relative enthalpies in kcal/mol. The geometry of the transition state was optimized using B3LYP/6-311++G(d,p) level of theory and was identified by the existence of single imaginary frequency from vibrational mode analysis. Single point energy refinement was performed by B3LYP, BMK, M05-2X, and M06-2X/6-311++G(3df,3pd) levels of theory, respectively. The presented reaction barriers include enthalpy corrections calculated by B3LYP/6-311++G(d,p) level of theory at 298.15K and 1 atm.

3.3.7. Disulfide Bond Cleavage by FRIPS versus ECD

As we discussed in the previous sections, the reaction mechanisms of FRIPS and ECD that lead to disulfide bond cleavage are different. However, the observed products from disulfide bond cleavage using FRIPS and ECD methods share a common feature by having the prominent products from S–S bond cleavage. On the other hand, ECD more prefers to cleave S–S bonds while FRIPS still fragments C–S bonds. The difference on relative abundances of the products from the C–S bond cleavage in each method could be partially attributed to the time scale of measurement. Considering the time scale of mass spectrometers used in this study (ion traps versus FT-ICR) in ion detection, the product distribution can be dominated by the lowest-energy pathway in longer time scale with a FT-ICR mass spectrometer. As a result, favored S–S bond cleavage fragments are prominent in ECD spectra whereas competitive C–S bond cleavage processes are observed in FRIPS spectra.

3.3.8. Reactivity of Disulfide Bond with Radicals

Both radical-driven peptide fragmentation methods, FRIPS and ECD produce abundant products from disulfide bond cleavage. It is also independent on its connectivity (*i.e.*, intra- or intermolecular linkages). The present experimental and theoretical results provide critical insights relating to selective disulfide bond cleavages effected using different experimental methodologies. Free-radical processes that cleave disulfide bonds in proteins are ubiquitous in nature,^{183,188} resulting from a wide range of redox reactions *in vivo* in addition to the environmental hazards of ionizing and UV radiation. We believe that mechanistic aspects of disulfide bond cleavage in nature can be better understood by our fundamental biomimetic studies of model systems using well-constrained hydrogen-rich and hydrogen-deficient conditions.

3.4. Conclusion

The mechanism of disulfide bond cleavage by a regiospecific acetyl radical (FRIPS) is investigated and compared to that of a low-energy electron (ECD). The second generation TEMPO-based FRIPS reagent is derivatized to model peptides to generate the regiospecific acetyl radical group via collisional activation that predominantly leads to loss of TEMPO radical. Following collisional activation of the acetyl radical attached model peptides yields highly selective C–S and S–S bond cleavages in both inter- and intradisulfide linkages. Additional collisional activations of fragments from C–S and S–S bond cleavages generate sequence information of disulfide-linked peptide chains, allowing us to assign disulfide bond linkages between cysteine residues. Both C–S and S–S bond cleavage processes are mainly initiated by H-abstraction at the α -carbons. Following β - and γ -cleavages lead to C–S and S–S bond cleavages. Density functional theory calculations reveal the energetics of the C–S and S–S bond cleavage processes. Other possibilities (direct radical substitution and hydrogen shift between the α - and β -carbons) for explanation on the favored S–S bond cleavage in FRIPS are also suggested and discussed. Observed gas-phase fragmentation pathways can provide insights on biological processes associated with disulfide bond cleavages by reactive radical species and redox stresses.

3.5. Acknowledgment

This work was supported by the National Science Foundation through grant CHE-0416381 and the Beckman Institute at California Institute of Technology. Electron capture dissociation was performed using the LTQ-FT in the Proteome Exploration Laboratory, the Beckman Institute.

Computational resources were kindly provided by the Materials and Process Simulation Center at California Institute of Technology. C.H.S. acknowledges a fellowship from the Kwanjeong Educational Foundation.

Supporting Information Available:

1. Peptide fragmentation nomenclature used in this study for c- and z-type ions produced by ECD and ETD versus a- and x-type ions produced by FRIPS.
2. Details on the synthesis of the TEMPO-based FRIPS reagent and peptide conjugation.
3. The precursor ion structure of TEMPO-CFIR/NCPR.